INTERNATIONAL JOURNAL FOR NUMERICAL METHODS IN FLUIDS
Int. J. Numer. Meth. Fluids 2009; **59**:239–257
Published online 8 November 2006 in Wiley InterScience (www.interscience.wiley.com). DOI: 10.1002/fld.1393

Discrete duality finite volume schemes for two-dimensional drift-diffusion and energy-transport models

C. Chainais-Hillairet*, †

Laboratoire de Mathématiques, UMR 6620, 24, avenue des Landais, Aubiere Cedex 63177, France

SUMMARY

The drift-diffusion and the energy-transport models appear in the modelling of semiconductor devices. The main difficulty arising in the approximation of the energy transport model by finite volume schemes is the discretization of the Joule heating term in the equation on the density of energy. Following some recent ideas by Domelevo and Omnès for the discretization of the Laplace equation on almost general meshes, we construct a finite volume approximation of the 2-D drift-diffusion and energy transport models. These schemes still hold on almost general meshes. Finally, we present numerical simulations of semiconductor devices. Copyright © 2006 John Wiley & Sons, Ltd.

Received 8 May 2006; Revised 25 September 2006; Accepted 30 September 2006

KEY WORDS: drift-diffusion; energy transport; finite volume; semiconductor device; diode; transistor

1. INTRODUCTION

In the modelling of semiconductor devices, two main classes of classical models can be distinguished: kinetic models and fluid dynamical models (for the presentation of the hierarchy of models, see for instance [1–3]). The drift-diffusion and the energy-transport models belong to the class of fluid dynamical models. Since they are coupled systems of parabolic and elliptic equations, they are well adapted for numerical simulations and particularly by finite volume methods.

1.1. The drift-diffusion model

The simplest model is the drift-diffusion system. It consists of two continuity equations for the density of charges (electrons and holes), coupled with the Poisson equation for the electrostatic

*Correspondence to: C. Chainais-Hillairet, Laboratoire de Mathématiques, UMR 6620, 24, avenue des Landais, 63177 Aubiere Cedex, France.
†E-mail: Claire.Chainais@math.univ-bpclermont.fr

Contract/grant sponsor: Publishing Arts Research Council; contract/grant number: 98-1846389

Copyright © 2006 John Wiley & Sons, Ltd.

potential. Let $\Omega \subset \mathbb{R}^2$ be an open and bounded polygonal domain describing the geometry of the semiconductor device, we set $\Gamma = \partial\Omega$, the boundary of the domain, and ν the unit outwards normal to Ω. If we set all physical constants to 1 for the sake of simplicity, the drift-diffusion system writes

$$\partial_t N - \operatorname{div}(J_N) = 0 \quad \text{in } \Omega \times]0, \tau[\quad \text{with } J_N = \nabla r(N) - N\nabla V \tag{1}$$

$$\partial_t P - \operatorname{div}(J_P) = 0 \quad \text{in } \Omega \times]0, \tau[\quad \text{with } J_P = \nabla r(P) + P\nabla V \tag{2}$$

$$\Delta V = N - P - C \quad \text{in } \Omega \times]0, \tau[\tag{3}$$

where $C(x)$ is the prescribed doping profile of the device and the nonlinear function r denotes the pressure of electrons and holes which behave like a gas (in the applications, $r(s) = s^\gamma$, with $\gamma = \frac{5}{3}$). Equations (1)–(3) are supplemented with initial conditions $(N^0,\ P^0)$ and boundary conditions. The physically motivated boundary conditions are mixed Dirichlet–Neumann boundary conditions: Dirichlet boundary conditions on the ohmic contacts, homogeneous Neumann boundary conditions on the insulating boundary segments. Therefore, the boundary Γ splits into two parts: $\Gamma = \Gamma^{\mathrm{D}} \cup \Gamma^{\mathrm{N}}$ and the boundary conditions are

$$N = \overline{N}, \quad P = \overline{P}, \quad V = \overline{V} \quad \text{on } \Gamma^{\mathrm{D}} \times\ ]0, \tau[$$

$$\nabla r(N) \cdot \nu = \nabla r(P) \cdot \nu = \nabla V \cdot \nu = 0 \quad \text{on } \Gamma^{\mathrm{N}} \times\ ]0, \tau[$$

A lot of numerical algorithms have already been proposed for solving this system. A review of exponentially fitted difference or finite element methods is presented in [4]: it refers to the first work by Scharfetter and Gummel [5] on exponentially fitted difference schemes in 1-D and also to more recent papers like [6–9]. In [10], we studied finite volume discretization for the multidimensional nonlinear drift-diffusion system. Using the techniques developed by Eymard *et al.* in [11], we proved the convergence of the finite volume scheme and then the existence of solutions to the nonlinear drift-diffusion system. Numerical simulations of the drift-diffusion system give physically relevant results for micrometer size devices.

1.2. The energy-transport model

However, the simple drift-diffusion system (1)–(3) is not accurate enough for sub-micron device modelling, owing to temperature effects and hot electrons. In this case, it is interesting to work with an energy transport model which takes into account the temperature effects and remains simpler than hydrodynamic equations or semiconductor Boltzmann equations because it can still be written in a drift-diffusion form. The energy transport models for semiconductor devices can be derived either from hydrodynamic models by neglecting certain convection terms [12] or from the Boltzmann equation by means of the Hilbert expansion method [13]. Here, we restrict our attention to the transient version of the Chen model derived in [14]. It consists of continuity equations for density of electrons N and density of energy U coupled with a Poisson equation for the electrostatic potential V. In the scaled variables, the system writes

$$\partial_t N - \operatorname{div}(J_N) = 0 \quad \text{in } \Omega \times\ ]0, \tau[\tag{4}$$

Copyright © 2006 John Wiley & Sons, Ltd.

DOI: 10.1002/fld

$$\partial_t U - \operatorname{div}(J_U) = -J_N \cdot \nabla V + W(N,U) \quad \text{in } \Omega \times]0,\tau[\tag{5}$$

$$\lambda^2 \Delta V = N - C \quad \text{in } \Omega \times]0,\tau[\tag{6}$$

where J_N and J_U are the current densities of charge and energy, $J_N \cdot \nabla V$ is the Joule heating term, $W(N,U)$ is the energy relaxation term, λ^2 is the Debye length and $C(x)$ is the prescribed doping profile of the device. The current densities are defined by

$$J_N = \nabla N - N\frac{\nabla V}{T}, \quad J_U = \nabla U - U\frac{\nabla V}{T}$$

In the Chen model, the densities N and U are linked with the temperature T by the relation

$$U = \tfrac{3}{2}NT$$

and the energy relaxation term is given by

$$W(N,U) = c_1 N - c_2 U$$

Equations (4)–(6) are supplemented with initial data N^0, U^0 and mixed Dirichlet–Neumann boundary conditions

$$N = \overline{N}, \quad U = \overline{U}, \quad V = \overline{V} \quad \text{on } \Gamma^{\mathrm{D}} \times]0,\tau[$$

$$J_N \cdot \nu = J_U \cdot \nu = \nabla V \cdot \nu = 0 \quad \text{on } \Gamma^{\mathrm{N}} \times]0,\tau[$$

The discretization of the energy-transport equations has already been studied in many papers: extensions of Scharfetter–Gummel schemes in [15], ENO schemes in [16], finite element schemes in [17, 18], high-order compact difference schemes in [19]. In [20], we proposed a finite volume scheme for the 1-D energy-transport system.

1.3. Goal of the paper

The principle of finite volume schemes lies on integration of conservation laws on control volumes (cells of the mesh) and then on a finite difference discretization of fluxes through the edges of the control volumes (edges of the mesh). By applying this method to Equation (4) or (6), we define approximations of J_N and ∇V only on the edges and only along the normal to the edges. This method does not provide any approximation of J_N and ∇V along the edges. Then, there is some lack of information and the discretization of the Joule heating term $J_N \cdot \nabla V$ (or more precisely $\int_K J_N \cdot \nabla V$ for a control volume K) is not straightforward.

In this paper, we propose a method which provides the reconstruction of discrete gradients and discrete currents on the whole domain and then a straightforward discretization of the Joule heating term. Therefore, we follow the ideas of Domelevo and Omnès [21] for the discretization of the Laplace equation and we adapt them to convection–diffusion equations. A reconstruction of the gradients proposed by Coudière *et al.* [22] is used and the principle of the scheme lies on integration of the equations on primal and dual cells as done by Hermeline [23, 24]. This method holds for the drift-diffusion and the energy-transport systems. It works on almost all general meshes.

Section 2 is devoted to the definition of discrete gradients and currents. It leads to a new scheme for the drift-diffusion and energy-transport models on almost all general meshes. In Section 3, numerical simulations of the drift-diffusion system (PN junction diode and PNP transistor) and the Chen energy-transport model (2-D ballistic diode) are shown.

Copyright © 2006 John Wiley & Sons, Ltd.

DOI: 10.1002/fld

2. CONSTRUCTION OF THE FINITE VOLUME SCHEME

2.1. Motivation and principle

The main works on finite volume schemes for elliptic or parabolic equations are based on a restrictive assumption on the mesh. Indeed, an admissible mesh of a domain Ω is given by a family $\mathscr{T}$ of control volumes, a family $\mathscr{E}$ of edges and a family $(x_K)_{K\in\mathscr{T}}$ of points such that the straight line between two neighbouring centres of cells (x_K, x_L) is orthogonal to the considered edge (see Definition 5.1 in [11]). Under this hypothesis, the following two points approximation of the flux ∇V through the interface σ_{KL} (K and L are two neighbouring cells), whose normal and measure are, respectively, denoted ν_{KL} and $m(\sigma_{KL})$, turns natural:

$$\int_{\sigma_{KL}} \nabla V \cdot \nu_{KL} \approx m(\sigma_{KL}) \frac{V_L - V_K}{d(x_K, x_L)}$$

In the same way, with an upwind discretization of the convective term, we have the following approximation for a current density like $J_N = \nabla N - (N/T)\nabla V$:

$$\int_{\sigma_{KL}} \nabla J_N \cdot \nu_{KL} \approx m(\sigma_{KL}) \frac{N_L - N_K}{d(x_K, x_L)} - m(\sigma_{KL}) \frac{V_L - V_K}{d(x_K, x_L)} \cdot \begin{cases} \dfrac{N_K}{T_K} & \text{if } V_L \geqslant V_K \\ \dfrac{N_L}{T_L} & \text{if } V_L \leqslant V_K \end{cases}$$

Therefore, the usual two point discretization of the gradient and the current density provide an approximation of the gradient ∇V and J_N only in the direction ν_{KL} orthogonal to the edge σ_{KL}, which seems not sufficient for the discretization of the Joule heating term $J_N \cdot \nabla V$.

In order to get a reconstruction of the gradients and the current densities, we will adapt the ideas developed by Domelevo and Omnès [21]. In this paper, the authors study a new finite volume method for the Laplace equation. This method lies on the reconstruction of approximate gradients using unknowns at the centres and the nodes of the mesh as proposed by Coudière *et al.* in [22]. The scheme comes from the integration of the Laplace equation on primal and dual control volumes. It provides a linear system with a symmetric positive definite matrix. If the mesh is admissible in the sense of Definition 5.1 in [11], the scheme splits into two separate schemes: the classical cell-centred scheme and the classical vertex-centred scheme.

The main advantages of this method are that it can be applied on almost all general meshes and that it provides a complete reconstruction of the gradients. Convergence of the scheme for the Laplace equation is established in [21]. Its main drawback is the size of the linear systems: indeed, the number of discrete unknowns is the sum of the number of cells and the number of nodes.

2.2. Mesh

In order to construct the scheme, we first have to describe the mesh of the domain. As in [21], three simultaneous meshes for the same domain are taken under consideration:

1. the primal mesh is for instance a triangulation of Ω;
2. the dual mesh is obtained by connecting all the centres of gravity of the primal cells and midpoints of the boundary edges;
3. the diamond mesh whose nodes are the nodes and the centres of the primal mesh.

Copyright © 2006 John Wiley & Sons, Ltd.

DOI: 10.1002/fld

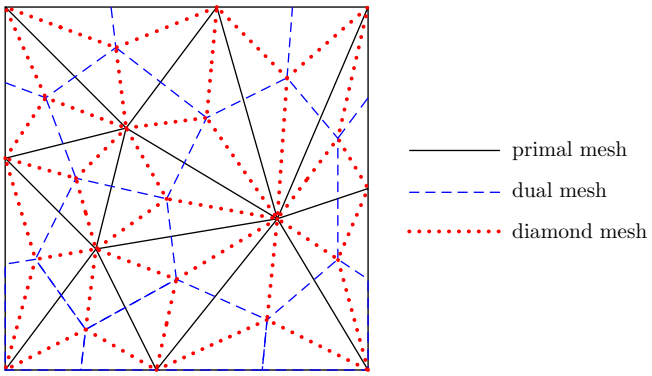

Figure 1. Presentation of the meshes.

The three meshes are presented in Figure 1. The notations are the following:

- $\mathcal{T}$ is a family of polygonal control volumes such that $\Omega = \bigcup_{K\in\mathcal{T}} K$, it defines the primal mesh.
- $\mathcal{P}$ is the family of nodes of the primal mesh, which can be split into $\mathcal{P} = \mathcal{P}^{\text{int}} \cup \mathcal{P}^{\text{D}} \cup \mathcal{P}^{\text{N}}$ where we distinguish the interior points, $\mathcal{P}^{\text{int}}$, the points belonging to Γ^{D}, $\mathcal{P}^{\text{D}}$, and the points belonging to Γ^{N}, $\mathcal{P}^{\text{N}}$.
- $\mathcal{E}$ is the family of edges of the primal mesh, which can be split into $\mathcal{E} = \mathcal{E}^{\text{int}} \cup \mathcal{E}^{\text{D}} \cup \mathcal{E}^{\text{N}}$ where we distinguish the interior edges, $\mathcal{E}^{\text{int}}$, the edges on Γ^{D}, $\mathcal{E}^{\text{D}}$, and the edges on Γ^{N}, $\mathcal{E}^{N}$.
- For any $P \in \mathcal{P}$, we define K_P the cell obtained by connecting the centres of the primal cells with vertex P and the midpoints of the boundary edges if $P \in \Gamma$. Then, we obtain a dual mesh of Ω since $\Omega = \bigcup_{P\in\mathcal{P}} K_P$.
- The set of the edges of the dual mesh is denoted $\widetilde{\mathcal{E}}$.
- For all $\sigma \in \mathcal{E}$, we define D_σ the diamond obtained by connecting the vertices of σ and the centres of the neighbouring cells (if σ is on the boundary, the diamond reduces to a triangle). Thus, we obtain a third mesh: the diamond mesh of Ω since $\Omega = \bigcup_{\sigma\in\mathcal{E}} D_\sigma$.
- For all $K \in \mathcal{T}$, x_K is the centre of gravity of K. For $\sigma \in \mathcal{E}$, if $\sigma \subset \partial K$, the unit normal to σ outwards K is denoted $\nu_{K,\sigma}$.
- For all $P \in \mathcal{P}$ and $\tilde{\sigma} \in \widetilde{\mathcal{E}}$, if $\tilde{\sigma} \in \partial K_P$, the unit normal to $\tilde{\sigma}$ outwards K_P is denoted $\nu_{K_P,\tilde{\sigma}}$.

2.3. *Reconstruction of the gradient*

Let us now recall the definition of the discrete gradient ∇^{d}, introduced in [21]. This operator is *a priori* defined for any vector Φ of known values at the centres and the nodes of the mesh and the midpoints of the boundary edges and gives a discrete gradient $\nabla^{\text{d}}\Phi$ which is piecewise constant on each diamond cell:

$$\nabla^{\text{d}} : \Phi \in \mathbb{R}^{|\mathcal{T}|+|\mathcal{P}|+|\mathcal{E}^{\text{D}}|+|\mathcal{E}^{\text{N}}|} \to \nabla^{\text{d}}\Phi \in (\mathbb{R}^{|\mathcal{E}|})^2$$

Here, we adapt the definition of ∇^{d} in order to take into account the boundary conditions.

Copyright © 2006 John Wiley & Sons, Ltd.

DOI: 10.1002/fld

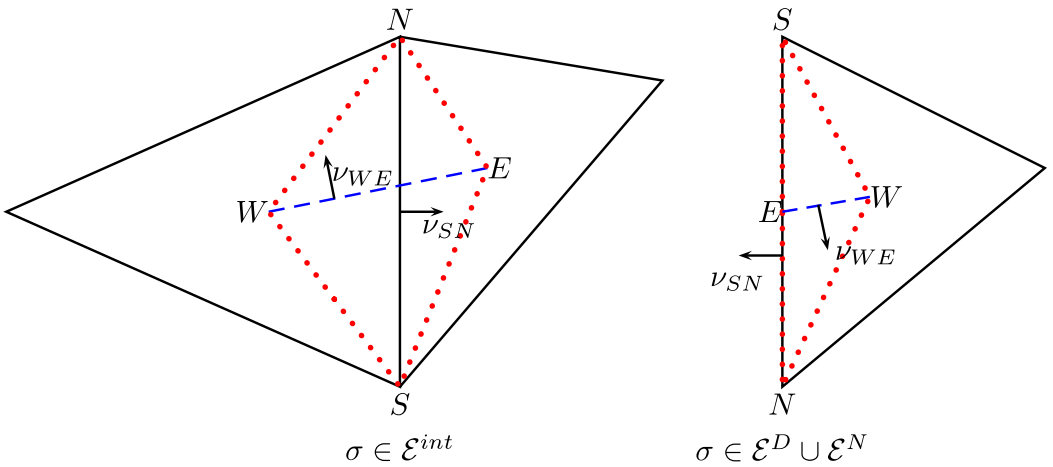

Figure 2. Notations for the reconstruction of the gradient.

Let us consider an edge of the primal mesh $\sigma \in \mathscr{E}$. If $\sigma \in \mathscr{E}^{\text{int}}$, we choose an orientation for σ such that its vertices are denoted S and N and the centres of the neighbouring cells W and E. The boundary Γ is oriented anticlockwise, such that, if $\sigma \in \mathscr{E}^{\text{D}} \cup \mathscr{E}^{\text{N}}$, the point W is inside the domain and the point E is on the boundary (we set $E = (N + S)/2$), see Figure 2.

The diamond D_σ is obtained by connecting the points N, W, S, E (if $\sigma \in \mathscr{E}^{\text{D}} \cup \mathscr{E}^{\text{N}}$, D_σ is confined to the triangle NWS). We set:

- $\mathbf{v}_{SN}$ the unit normal to $[SN]$ oriented from W to E;
- $\mathbf{v}_{WE}$ the unit normal to $[WE]$ oriented from S to N;
- SN the length of $[SN]$;
- WE the length of $[WE]$;
- A_σ the area of D_σ.

Then, given Φ_N, Φ_S, Φ_E, Φ_W, the values of Φ at the points N, S, E, W, $\nabla^{\text{d}}\Phi$ is defined on D_σ by

$$\nabla^{\text{d}}\Phi_{|D_\sigma} = \frac{1}{2A_\sigma}((\Phi_E - \Phi_W)SN\mathbf{v}_{SN} + (\Phi_N - \Phi_S)WE\mathbf{v}_{WE}) \quad \forall \sigma \in \mathscr{E} \cup \mathscr{E}^{\text{D}} \tag{7}$$

In the sequel, some values of Φ will be unknowns of the scheme and some others will be given by the boundary conditions. In particular, if $\sigma \in \mathscr{E}^{\text{N}}$, the boundary condition $\nabla^{\text{d}}\Phi_{|D_\sigma} \cdot \mathbf{v}_{SN} = 0$ yields

$$\nabla^{\text{d}}\Phi_{|D_\sigma} = \frac{1}{2A_\sigma}(\Phi_N - \Phi_S)WE(\mathbf{v}_{WE} - \mathbf{v}_{SN} \cdot \mathbf{v}_{WE}\mathbf{v}_{SN}) \quad \forall \sigma \in \mathscr{E}^{\text{N}} \tag{8}$$

Furthermore, it will happen that one or the two vertices of an edge σ belong to Γ^{D}. In this case, the corresponding values Φ_N or Φ_S are prescribed by the boundary conditions:

$$\Phi_N = \overline{\Phi}(N) \quad \text{if } N \in \mathscr{P}^{\text{int}}, \quad \Phi_S = \overline{\Phi}(S) \quad \text{if } S \in \mathscr{P}^{\text{int}} \tag{9}$$

Copyright © 2006 John Wiley & Sons, Ltd.

DOI: 10.1002/fld

If N and S are both in $\mathscr{P}^{\text{int}}$, then we define Φ_E by

$$\Phi_E = \frac{\overline{\Phi}(S) + \overline{\Phi}(N)}{2} \quad \forall \sigma \in \mathscr{E}^{\text{D}} \tag{10}$$

Finally, the operator ∇^{d} is defined from $\mathbb{R}^{|\mathscr{T}|+|\mathscr{P}^{\text{int}}|+|\mathscr{P}^{\text{N}}|}$ to $(\mathbb{R}^{|\mathscr{E}|})^2$ by (7)–(10).

2.4. *Reconstruction of the current densities*

As for the gradient, we now define some reconstruction of the current densities. The current densities in the drift-diffusion system write $J_N = \nabla r(N) - N\nabla V$ and $J_P = \nabla r(P) + P\nabla V$ and in the energy-transport system, they write $J_N = \nabla N - (N/T)\nabla V$ and $J_U = \nabla U - (U/T)\nabla V$. In both cases, the current densities are made of a diffusion part and a convection part. In order to have some general definition for the approximate current densities, we use a general compact form for the current density:

$$\mathscr{J}(\Phi, \Psi, \Pi) = \nabla\Phi - \Psi\nabla\Pi$$

Thus, for the drift-diffusion system, we have

$$J_N = \mathscr{J}(r(N), N, V) \quad \text{and} \quad J_P = \mathscr{J}(r(P), -P, V)$$

and for the energy-transport system, we have

$$J_N = \mathscr{J}\left(N, \frac{N}{T}, V\right) \quad \text{and} \quad J_U = \mathscr{J}\left(U, \frac{U}{T}, V\right)$$

As the discrete gradient ∇^{d}, the discrete current density $\mathscr{J}^{\text{d}}$ is a discrete operator:

$$\mathscr{J}^{\text{d}} : (\Phi, \Psi, \Pi) \in (\mathbb{R}^{|\mathscr{T}|+|\mathscr{P}^{\text{int}}|+|\mathscr{P}^{\text{N}}|})^3 \to \mathscr{J}^{\text{d}}(\Phi, \Psi, \Pi) \in (\mathbb{R}^{|\mathscr{E}|})^2$$

It can be defined by its scalar products $\mathscr{J}^{\text{d}}(\Phi, \Psi, \Pi)_{|D_\sigma} \cdot \mathbf{v}_{SN}$ and $\mathscr{J}^{\text{d}}(\Phi, \Psi, \Pi)_{|D_\sigma} \cdot \mathbf{v}_{WE}$. These scalar products are the relevant quantities on each diamond D_σ for the construction of the scheme. Indeed, the scheme will be obtained after integration of the constitutive equations on the primal and the dual cells. But in the diamond D_σ, the diagonal SN is an edge of the primal mesh, while the diagonal WE is an edge of the dual mesh (see Figure 2 for the notations). Therefore, in the construction of the scheme, we need to approximate $\int_{SN} \mathscr{J} \cdot \mathbf{v}_{SN}$ and $\int_{WE} \mathscr{J} \cdot \mathbf{v}_{WE}$.

As $\mathscr{J}$ contains a convective part, it is classical to use an upwind discretization for this convective part $\Psi\nabla\Pi$. Therefore, we just consider that for the SN edge the upstream point is W and the downstream point is E, while for the WE edge the upstream point is S and the downstream point is N. It leads to the following definition:

$$\begin{aligned}\mathscr{J}^{\text{d}}(\Phi, \Psi, \Pi)_{|D_\sigma} \cdot \mathbf{v}_{SN} &= \nabla^{\text{d}}\Phi \cdot \mathbf{v}_{SN} - (\nabla^{\text{d}}\Pi \cdot \mathbf{v}_{SN})^+ \Psi_W - (\nabla^{\text{d}}\Pi \cdot \mathbf{v}_{SN})^- \Psi_E \quad \forall \sigma \in \mathscr{E}^{\text{int}} \cup \mathscr{E}^{\text{D}} \\ &= 0 \quad \forall \sigma \in \mathscr{E}^{\text{N}}\end{aligned}$$

$$\mathscr{J}^{\text{d}}(\Phi, \Psi, \Pi)_{|D_\sigma} \cdot \mathbf{v}_{WE} = \nabla^{\text{d}}\Phi \cdot \mathbf{v}_{WE} - (\nabla^{\text{d}}\Pi \cdot \mathbf{v}_{WE})^+ \Psi_S - (\nabla^{\text{d}}\Pi \cdot \mathbf{v}_{WE})^- \Psi_N \quad \forall \sigma \in \mathscr{E}$$

where $x^+ = \max(x, 0)$ and $x^- = \min(x, 0)$.

Copyright © 2006 John Wiley & Sons, Ltd.

DOI: 10.1002/fld

This is a compact definition for the approximate current densities. Let us just note that, in practice, the approximate current density $\mathscr{J}^{\mathrm{d}}(\Phi, \Psi, \Pi)$ can be expressed on each diamond D_σ as a combination of the values of Φ, Ψ and Π at the four vertices of the diamond (N, S, W, E), for instance in the non-orthogonal basis $\mathbf{v}_{SN}$, $\mathbf{v}_{WE}$.

2.5. Numerical scheme for the energy-transport model

We just present the numerical scheme for the energy-transport model. Indeed, the scheme is exactly the same for the drift-diffusion system with the corresponding current densities and without any source term in the conservation equations.

Let Δt be the time step and $t^n = n\Delta t$. In general for finite volume methods, the unknowns are localized either at the centres or at the vertices of the control volumes. Here, the unknowns are the values of N, U, V at time t^n at the centres of the mesh:

$$N_K^n,\ U_K^n,\ V_K^n \quad \forall K \in \mathscr{T}\ \ \forall n \geqslant 0$$

and also at the nodes of the mesh

$$N_P^n,\ U_P^n,\ V_P^n \quad \forall P \in \mathscr{P}\ \ \forall n \geqslant 0$$

and the unknown vectors at time t^n are denoted by

$$N^n = ((N_K^n)_{K\in\mathscr{T}}, (N_P^n)_{P\in\mathscr{P}}), \quad U^n = ((U_K^n)_{K\in\mathscr{T}}, (U_P^n)_{P\in\mathscr{P}}), \quad V^n = ((V_K^n)_{K\in\mathscr{T}}, (V_P^n)_{P\in\mathscr{P}})$$

First, we discretize initial and boundary data and the doping profile

$$N_K^0 = \frac{1}{m(K)}\int_K N^0, \quad U_K^0 = \frac{1}{m(K)}\int_K U^0 \quad \forall K \in \mathscr{T}$$

$$N_P^0 = \frac{1}{m(K_P)}\int_{K_P} N^0, \quad U_P^0 = \frac{1}{m(K_P)}\int_{K_P} U^0 \quad \forall P \in \mathscr{P}^{\mathrm{int}} \cup \mathscr{P}^{\mathrm{N}}$$

$$N_P^n = \overline{N}(P, t^n), \quad U_P^n = \overline{U}(P, t^n), \quad V_P^n = \overline{V}(P, t^n) \quad \forall P \in \mathscr{P}^{\mathrm{D}} \quad \forall n \geqslant 0$$

$$C_K = \frac{1}{m(K)}\int_K C \quad \forall K \in \mathscr{T}, \quad C_P = \frac{1}{m(K_P)}\int_{K_P} C \quad \forall P \in \mathscr{P}$$

The scheme on V writes

$$\sum_{\sigma\subset\partial K}\int_\sigma \nabla^{\mathrm{d}} V^n \cdot \nu_{K,\sigma} = m(K)(N_K^n - C_K) \quad \forall K \in \mathscr{T} \tag{11}$$

$$\sum_{\tilde{\sigma}\subset\partial K_P}\int_{\tilde{\sigma}} \nabla^{\mathrm{d}} V^n \cdot \nu_{K_P,\tilde{\sigma}} = m(K_P)(N_P^n - C_P) \quad \forall P \in \mathscr{P}^{\mathrm{int}} \cup \mathscr{P}^{\mathrm{N}} \tag{12}$$

Copyright © 2006 John Wiley & Sons, Ltd.

DOI: 10.1002/fld

For N, the scheme is Euler explicit in time:

$$m(K)\frac{N_K^{n+1}-N_K^n}{\Delta t}-\sum_{\sigma\subset\partial K}\int_\sigma \mathscr{J}^{\mathrm{d}}\left(N^n,\frac{N^n}{T^n},V^n\right)\cdot v_{K,\sigma}=0\quad\forall K\in\mathscr{T} \tag{13}$$

$$m(K_P)\frac{N_P^{n+1}-N_P^n}{\Delta t}-\sum_{\tilde\sigma\subset\partial K_P}\int_{\tilde\sigma} \mathscr{J}^{\mathrm{d}}\left(N^n,\frac{N^n}{T^n},V^n\right)\cdot v_{K_P,\tilde\sigma}=0\quad\forall P\in\mathscr{P}^{\mathrm{int}}\cup\mathscr{P}^{\mathrm{N}} \tag{14}$$

For U, the current densities and the heating Joule term are discretized in an explicit way while the relaxation term is discretized in an implicit way:

$$\begin{aligned}&m(K)\frac{U_K^{n+1}-U_K^n}{\Delta t}-\sum_{\sigma\subset\partial K}\int_\sigma \mathscr{J}^{\mathrm{d}}(U^n,\frac{U^n}{T^n},V^n)\cdot v_{K,\sigma}\\&\quad=-\int_K \mathscr{J}^{\mathrm{d}}(U^n,\frac{U^n}{T^n},V^n)\cdot\nabla^{\mathrm{d}}V^n+m(K)(c_1N_K^{n+1}-c_2U_K^{n+1})\quad\forall K\in\mathscr{T}\end{aligned} \tag{15}$$

$$\begin{aligned}&m(K_P)\frac{U_P^{n+1}-U_P^n}{\Delta t}-\sum_{\tilde\sigma\subset\partial K_P}\int_{\tilde\sigma} \mathscr{J}^{\mathrm{d}}\left(U^n,\frac{U^n}{T^n},V^n\right)\cdot v_{K_P,\tilde\sigma}\\&\quad=-\int_{K_P} \mathscr{J}^{\mathrm{d}}\left(U^n,\frac{U^n}{T^n},V^n\right)\cdot\nabla^{\mathrm{d}}V^n+m(K_P)(c_1N_P^{n+1}-c_2U_P^{n+1})\quad\forall P\in\mathscr{P}^{\mathrm{int}}\cup\mathscr{P}^{\mathrm{N}}\end{aligned} \tag{16}$$

Equations (11), (13), (15) derive from integration of Equations (4)–(6) on the primal cells; Equations (12), (14), (16) come from integration on the dual cells.

At each time step, approximate densities of charge and energy N^n and U^n are computed explicitly and then the approximate potential V^n is obtained after resolution of a linear system. As established in [21], the matrix of this system is symmetric positive definite. Its size is the sum of the number of cells and the number of 'non-Dirichlet' points. At each time step, we also reconstruct the approximate gradient of V and the approximate current densities of charge and energy.

3. NUMERICAL EXPERIMENTS

In this section, we present numerical results obtained with our scheme.

Sections 3.1 and 3.2 are devoted to the simulation of a PN-diode and a PNP-transistor modelized by the drift-diffusion system. For this system, we proved in [10] the convergence of a 'classical' finite volume scheme under the assumption of admissibility of the mesh. The advantage of the scheme proposed here is that it works on more general meshes. The physical data in the test cases are given by Jüngel and Pietra [9].

In Section 3.3, we present the simulation of a 2-D-ballistic diode modelized by the Chen energy-transport model. The physical data are given by Holst *et al.* [18].

Copyright © 2006 John Wiley & Sons, Ltd.

DOI: 10.1002/fld

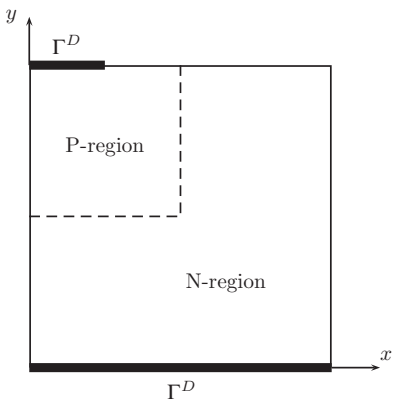

Figure 3. Geometry of the *PN*-junction diode.

Table I. Physical parameters for the silicon.

Parameter	Physical meaning	Numerical value
q	elementary charge	10^{-19} A s
ε	permittivity constant	10^{-12} A s V^{-1} cm^{-1}
n_i	intrinsic number	10^{10} cm^{-3}
μ_0	low field mobility	1.5×10^3 cm^2 V^{-1} s^{-1}
U_T	thermal voltage at $T_0 = 300$ K	0.0259 V
τ_0	energy relaxation time	0.4×10^{-12} s

3.1. Simulation of a PN-diode

The first numerical test is devoted to the simulation of a silicon *PN*-diode. The geometry of the device is shown in Figure 3. It is assumed to be a square of side $l = 10^{-3}$ cm. The pressure function has the form $r(s) = s^\gamma$ with $\gamma = \frac{5}{3}$. The numerical values of the physical parameters are given in Table I.

For a doping profile of size $\|C\|_\infty$, we set

$$\alpha = \frac{\gamma}{\gamma - 1}, \quad \beta = \left(\frac{n_i}{\|C\|_\infty}\right)^{\gamma - 1}, \quad U_0 = \frac{1}{2\alpha(1-\beta)}$$

The Debye length λ^2 is given by

$$\lambda^2 = \frac{\varepsilon V_\mathrm{b} U_0}{q l^2 \|C\|_\infty}$$

where V_b is the built-in potential of the device. When it is scaled by the unit scaling (see [4]), the scaled drift-diffusion system writes

$$\partial_t N - U_0 \operatorname{div}(\nabla(N^\gamma) - N \nabla V) = 0 \quad \text{in }]0,1[^2 \times]0, T[\tag{17}$$

Copyright © 2006 John Wiley & Sons, Ltd.

DOI: 10.1002/fld

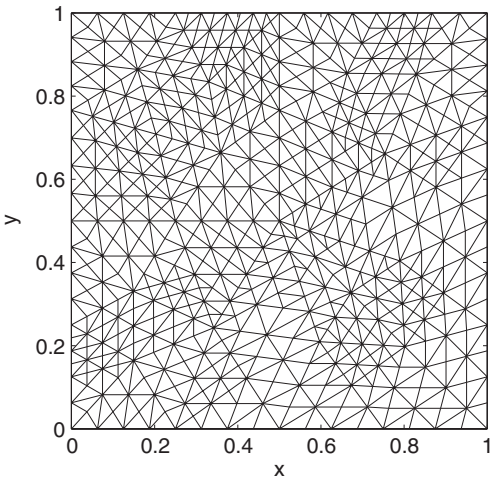

Figure 4. Distorted mesh for the *PN*-diode.

$$\partial_t P - U_0 \operatorname{div}(\nabla(P^\gamma) + P\nabla V) = 0 \quad \text{in }]0,1[^2 \times]0,T[\tag{18}$$

$$\lambda^2 \Delta V(x,t) = N - P - C \quad \text{in }]0,1[^2 \times]0,T[\tag{19}$$

with a piecewise constant dimensionless doping profile

$$C = -1 \quad \text{in the } P\text{-region}$$

$$C = 1 \quad \text{in the } N\text{-region}$$

and the boundary conditions

$$\overline{N} = 1, \quad \overline{P} = 0 \text{ at the contact of an } N\text{-region}$$

$$\overline{N} = 0, \quad \overline{P} = 1 \text{ at the contact of a } P\text{-region}$$

The boundary potential $\overline{V}$ will be given in each case as the superposition of the equilibrium potential and an applied voltage U:

$$\overline{V} = -\alpha(1-\beta) \quad \text{at the contact of the } P\text{-region}$$

$$\overline{V} = \alpha(1-\beta) - \frac{U}{V_b U_0} \quad \text{at the contact of the } N\text{-region}$$

3.1.1. A reverse biased diode. We first consider the case of a reverse biased diode. The moderate doping profile satisfies $\|C\|_\infty = 10^{15}\,\mathrm{cm}^{-3}$ and the built-in potential is $V_b = 0.5756\,\mathrm{V}$. We present in Figure 5 the results obtained for a strongly reverse biased diode with $U = -2.0\,\mathrm{V}$, when the steady state is reached. We compute the scaled N, P and V by two different methods: with the classical scheme proposed in [10] on an admissible mesh made of 947 triangles and 510 nodes and with the new scheme on the distorted mesh made of 1000 triangles and 537 nodes presented in

Copyright © 2006 John Wiley & Sons, Ltd.

DOI: 10.1002/fld

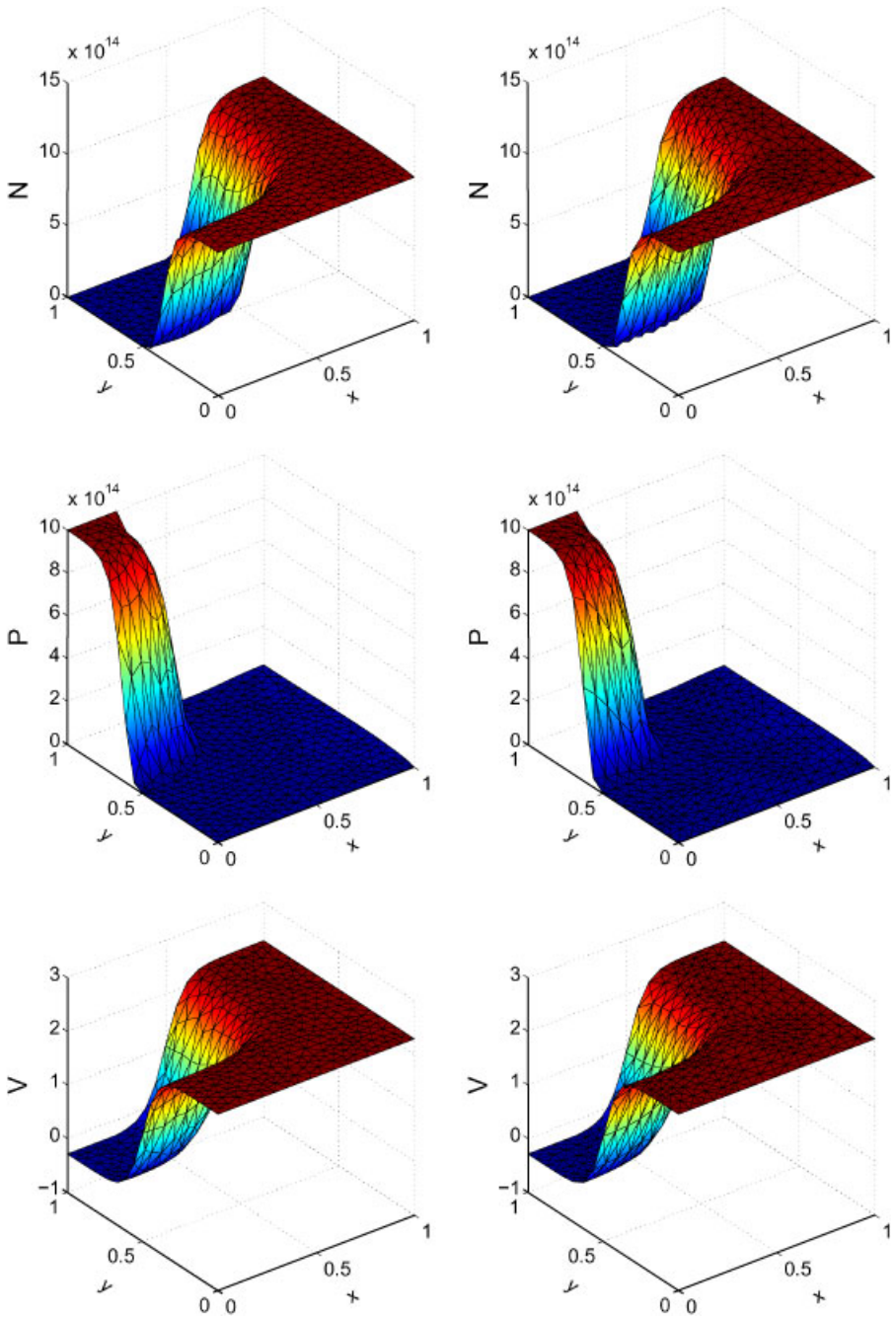

Figure 5. Reverse biased diode: $U = -2.0$ V, $\|C\|_\infty = 10^{15}$ cm^{-3}. Results obtained with the 'classical' scheme (on the left) and with the new scheme on the distorted mesh (on the right).

Copyright © 2006 John Wiley & Sons, Ltd.

DOI: 10.1002/fld

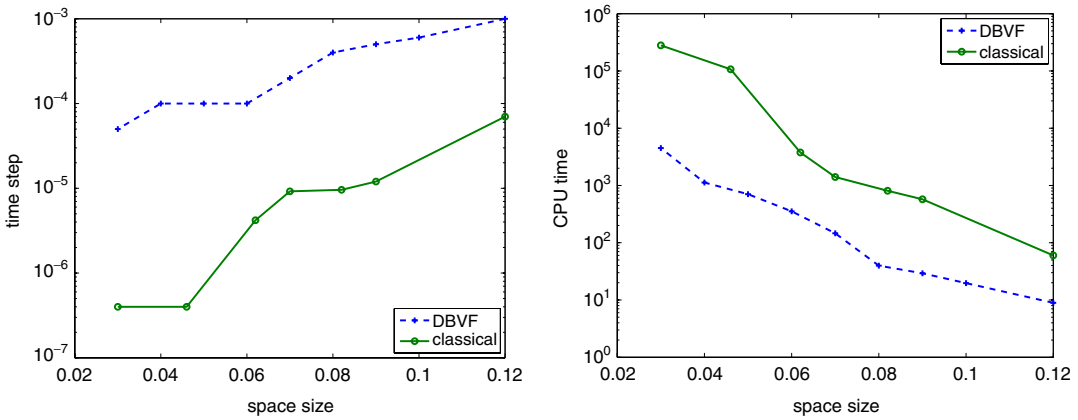

Figure 6. Case 1. Time step (on the left) and CPU time (on the right) for both schemes.

Figure 4. In this case, vacuum sets occur for the electron and hole densities; therefore, no current flows through the diode.

We obtain the same profiles with the two schemes. The results also allow for comparison with the results in [9] (steady-state case).

Both schemes are explicit in time. We present in Figure 6 the time step authorized for the computations and the time of computation required for the numerical solution of the first test case for both schemes (the classical one and the new one called 'DBVF'). We note that the time steps authorized are bigger for the new scheme than for the classical one. Therefore, though the linear systems inverted at each time step are bigger with the new scheme, the times of computations remain much smaller.

3.1.2. A forward biased diode. We now consider the case of a forward biased diode. The geometry of the device is shown in Figure 3. The computations are carried out with a doping profile satisfying $\|C\|_\infty = 10^{16}\,\mathrm{cm}^{-3}$, a built-in potential $V_\mathrm{b} = 0.6907\,\mathrm{V}$ and an applied voltage $U = 0.8\,\mathrm{V}$. We still compute N, P and V at the steady state by two different methods: with the classical scheme proposed in [10] on an admissible mesh made of 947 triangles and 510 nodes and with the new scheme on the distorted mesh made of 1000 triangles and 537 nodes presented in Figure 4. The results are given in Figure 7. In this case, we see that the vacuum sets for N and P are trivial and, therefore, current flows through the diode.

Figure 8 presents the time step authorized for the computations and the time required for the computation of the numerical solution in the second test case. We note that the time steps are not exactly the same as for the first test case. But the behaviour of the time step and the central processing unit (CPU) time *versus* the size of the mesh remain the same: the times of computation are smaller with the new scheme.

3.2. Simulation of the PNP-transistor

Now, we apply the numerical simulation of the scaled drift-diffusion system (17)–(19) to a PNP-transistor. The geometry of the device is shown in Figure 9. The moderate doping profile satisfies

Copyright © 2006 John Wiley & Sons, Ltd.

DOI: 10.1002/fld

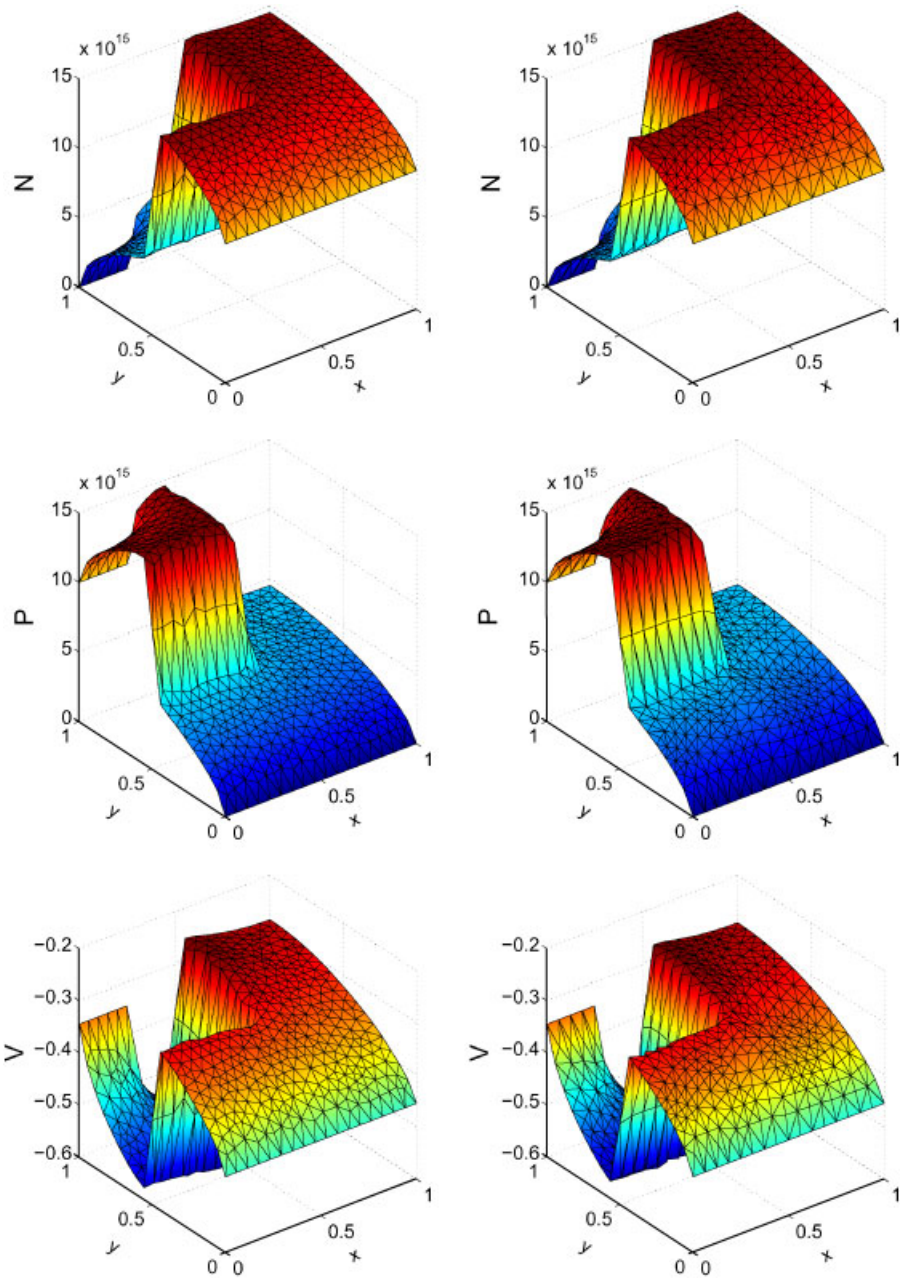

Figure 7. Forward biased diode: $U = 0.8$ V, $\|C\|_\infty = 10^{16}$ cm^{-3}. Results obtained with the 'classical' scheme (on the left) and with the new scheme on the distorted mesh (on the right).

Copyright © 2006 John Wiley & Sons, Ltd.

DOI: 10.1002/fld

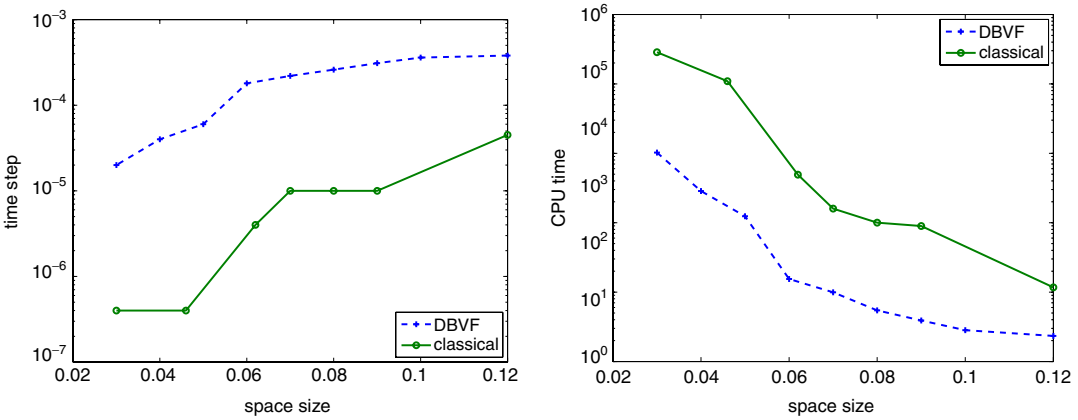

Figure 8. Case 2. Time step (on the left) and CPU time (on the right) for both schemes.

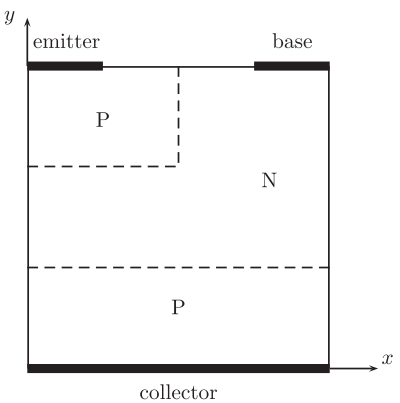

Figure 9. Geometry of the PNP-transistor.

$\|C\|_\infty = 10^{15}$ cm^{-3}, the built-in potential is $V_\mathrm{b} = 0.5756$ V and the boundary conditions for the electrostatic potential are

$$\overline{V} = 0 \quad \text{at the emitter}$$

$$\overline{V} = \frac{U_\mathrm{B}}{V_\mathrm{b} U_0} \quad \text{at the base}$$

$$\overline{V} = \frac{U_\mathrm{C}}{V_\mathrm{b} U_0} \quad \text{at the collector}$$

where $U_\mathrm{B} = -1.0$ V is the base potential and $U_\mathrm{C} = -2.0$ V is the collector potential.

Copyright © 2006 John Wiley & Sons, Ltd.

DOI: 10.1002/fld

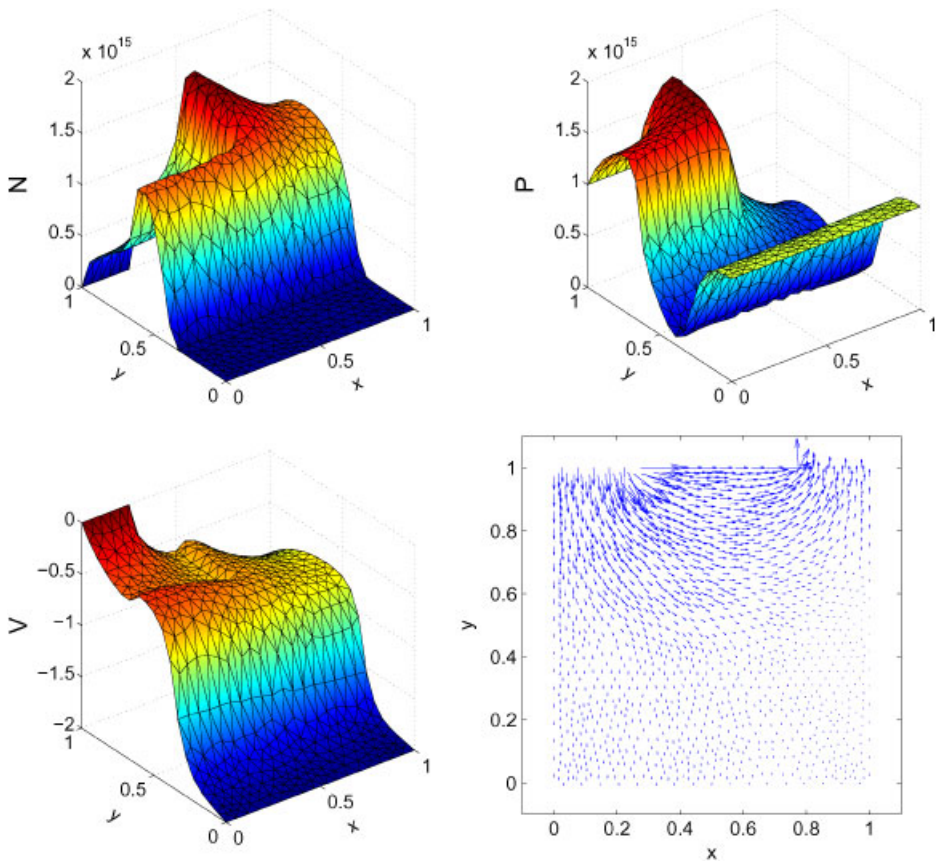

Figure 10. PNP-transistor: carrier densities, electrostatic potential and total current density.

The mesh of the domain contains 933 triangles and 504 nodes. We still compute the carrier densities and the electrostatic potential at the steady state. We also compute the total current density inside the transistor. The results are depicted Figure 10.

3.3. Simulation of the 2-D ballistic diode

We now present the simulation of a 2-D ballistic n^+nn^+ silicon diode which is uniform in one space dimension. The numerical results can be compared to the results in [17, 19] in 1-D and in [18] in 2-D.

The semiconductor domain is $\Omega = (0, l_x) \times (0, l_y)$ where $l_x = 0.6$ μm and $l_y = 0.2$ μm and the length of the channel equals 0.4 μm. It is presented in Figure 11. The numerical values of the physical parameters are given in Table I.

The doping profile is

$$C = C_m = 5 \times 10^{17}\ \text{cm}^{-3} \quad \text{in the } n^+ \text{ region}$$

$$C = C_n = 2 \times 10^{15}\ \text{cm}^{-3} \quad \text{in the } n \text{ region (channel)}$$

Copyright © 2006 John Wiley & Sons, Ltd.

DOI: 10.1002/fld

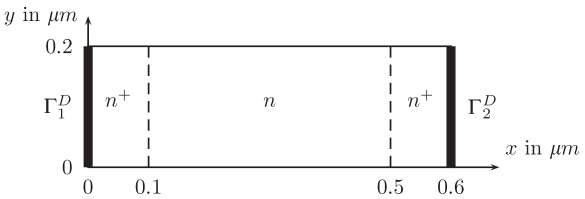

Figure 11. Geometry of the ballistic diode.

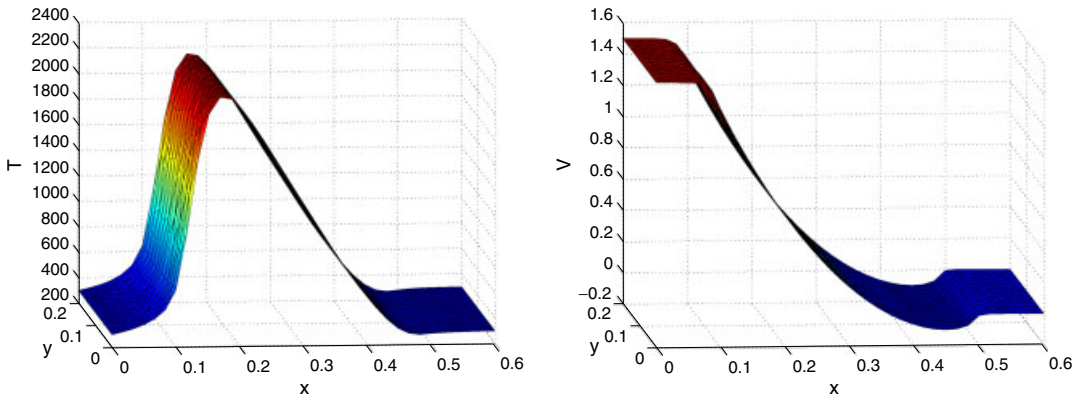

Figure 12. 2-D ballistic diode: temperature and electrostatic potential.

On the ohmic contacts, the boundary conditions are given by

$$N = C_m, \quad T = T_0, \quad V = U \quad \text{on } \Gamma_1^{\mathrm{D}}$$
$$N = C_m, \quad T = T_0, \quad V = 0 \quad \text{on } \Gamma_2^{\mathrm{D}}$$

where $T_0 = 300\,\mathrm{K}$ is the ambient temperature and $U = 1.5\,\mathrm{V}$ is the applied voltage. The coefficients c_1 and c_2 are given by

$$c_1 = \frac{3}{2}\frac{l_x^2}{\tau_0 \mu_0 U_T}, \quad c_2 = \frac{l_x^2}{\tau_0 \mu_0 U_T}$$

In Figure 12, we present the numerical results (temperature and electrostatic potential) for a non-uniform mesh with 1236 triangles and 666 nodes. As expected, the computed quantities are almost uniform in one space direction and we can see the hot electron effect in the channel.

In Figure 13, we recall the numerical results (temperature and electrostatic potential) obtained with the scheme proposed in [20] for the 1-D case.

Copyright © 2006 John Wiley & Sons, Ltd.

DOI: 10.1002/fld

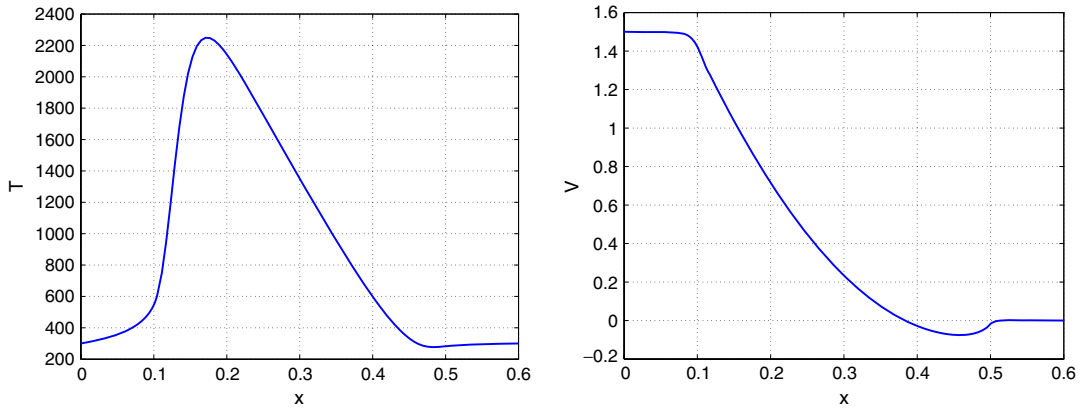

Figure 13. 1-D ballistic diode: temperature and electrostatic potential.

4. CONCLUSION

In this paper, we have developed a finite volume method for the drift-diffusion and the energy-transport systems. The scheme is an extension of the discrete duality finite volume scheme by Domelevo and Omnès to systems with convection–diffusion equations. One advantage of the discrete duality finite volume scheme is that it provides full discrete gradients and currents and, therefore, leads to a natural discretization of the Joule heating term.

We first showed different numerical simulations in the case of the drift-diffusion system. In this case, we can compare the efficiency of the new scheme with the 'classical' scheme proposed by Chainais-Hillairet and Peng [10]. It appears that the times of computations are smaller with the new scheme because it allows bigger time step. Furthermore, the new scheme works on almost all general meshes. Then, we showed that the new scheme provides the expected profiles for the simulation of the energy-transport system with the data of the 2-D ballistic diode.

REFERENCES

1. Jüngel A. *Quasi-Hydrodynamic Semiconductor Equations*. Birkhäuser: Basel, 2001.
2. Markowich PA, Ringhofer CA, Schmeiser C. *Semiconductor Equations*. Springer: Berlin, 1990.
3. Jerome JW. *Analysis of Charge Transport*. Springer: Berlin, 1996.
4. Brezzi F, Marini LD, Micheletti S, Pietra P, Sacco R, Wang S. Finite element and finite volume discretizations of drift-diffusion type fluid models for semiconductors. In *Handbook of Numerical Analysis*, vol. XIII, Numerical Methods for Electrodynamic Problems. Elsevier Science, 2005.
5. Scharfetter DL, Gummel HK. Large signal analysis of a silicon Read diode oscillator. *IEEE Transactions on Electron Devices* 1969; **ED-16**:64–77.
6. Brezzi F, Marini LD, Pietra P. Méthodes d'éléments finis mixtes et schéma de Scharfetter-Gummel. *Comptes Rendus de l' Academie des Sciences Paris Serie I-Mathematique* 1987; **305**:599–604.
7. Brezzi F, Marini LD, Pietra P. Numerical simulation of semiconductor devices. *Computer Methods in Applied Mechanics and Engineering* 1989; **75**:493–514.
8. Jüngel A. Numerical approximation of a drift-diffusion model for semiconductors with nonlinear diffusion. *Zeitschrift fur Angewandte Mathematik und Mechanik* 1995; **75**:783–799.
9. Jüngel A, Pietra P. A discretization scheme for a quasi-hydrodynamic semiconductor model. *Mathematical Models and Methods in Applied Sciences* 1997; **7**:935–955.

Copyright © 2006 John Wiley & Sons, Ltd.

DOI: 10.1002/fld

10. Chainais-Hillairet C, Peng Y-J. Finite volume approximation for degenerate drift-diffusion system in several space dimensions. *Mathematical Models and Methods in Applied Sciences* 2004; **14**(3):461–481.
11. Eymard R, Gallouët T, Herbin R. *Finite Volume Methods*. Handbook of Numerical Analysis, vol. VII. North-Holland: Amsterdam, 2000; 713–1020.
12. Gasser I, Natalini R. The energy-transport and the drift-diffusion equations as relaxation limits of the hydrodynamic models for semiconductors. *Quarterly of Applied Mathematics* 1999; **57**:269–282.
13. Ben Abdallah N, Degond P. On a hierarchy of macroscopic models for semiconductors. *Journal of Mathematical Physics* 1996; **37**:3308–3333.
14. Chen D, Kan E, Ravaioli U, Shu C-W, Dutton R. An improved energy transport model including nonparabolicity and non-Maxwellian distribution effects. *IEE Electron Device Letters* 1992; **13**(1):26–28.
15. Souissi K, Odeh F, Tang H, Gnudi A. Comparative studies of hydrodynamic and energy transport models. *COMPEL-The International Journal for Computation and Mathematics in Electrical and Electronic Engineering* 1994; **13**(2):439–453.
16. Jerome JW, Shu CW. Energy transport systems for semiconductors: analysis and simulation. *World Congress of Nonlinear Analysis*, vol. I–IV. de Gruyter: Berlin, 1996; 3835–3846.
17. Degond P, Jüngel A, Pietra P. Numerical discretization of energy-transport models for semiconductors with nonparabolic band structure. *SIAM Journal on Scientific Computing* 2000; **22**(3):986–1007.
18. Holst S, Jüngel A, Pietra P. A mixed finite-element discretization of the energy-transport model for semiconductors. *SIAM Journal on Scientific Computing* 2003; **24**(6):2058–2075.
19. Fournié M. Numerical discretization of the energy-transport model for semiconductors. *Applied Mathematics Letters* 2002; **15**(6):721–726.
20. Chainais-Hillairet C, Peng Y-J. Finite volume scheme for semiconductor energy-transport model. *Progress in Nonlinear Differential Equations and Their Applications*, vol. 63. 2005; 139–146.
21. Domelevo K, Omnès P. A finite volume method for the Laplace equation on almost arbitrary two-dimensional grids. *M2AN* 2005; **39**(6):1203–1249.
22. Coudière Y, Vila J-P, Villedieu P. Convergence rate of a finite volume scheme for a two dimensional convection diffusion problem. *M2AN* 1999; **33**(3):493–516.
23. Hermeline F. A finite volume method for the approximation of diffusion operators on distorted meshes. *Journal of Computational Physics* 2000; **160**:481–499.
24. Hermeline F. Approximation of diffusion operators with discontinuous coefficients on distorted meshes. *Computer Methods in Applied Mechanics and Engineering* 2003; **192**:1939–1959.

Copyright © 2006 John Wiley & Sons, Ltd.

DOI: 10.1002/fld